2024 IEEE/RSJ International Conference on Intelligent Robots and Systems (IROS)
October 14-18, 2024. Abu Dhabi, UAE

Soft finger rotational stability for precision grasps

Hun Jang[1*], Valentyn Petrichenko[1*], Joonbum Bae[2], Kevin Haninger[1]

***Abstract*—Soft robotic fingers can safely grasp fragile or variable form objects, but their force capacity is limited, especially with less contact area: precision grasps and when objects are smaller or not spherical. Although most research focuses on improving force capacity through mechanical design modifications, optimizing grasping parameters for precision tasks remains crucial. To address this problem, this paper proposes an analytical rotational stability model for soft fingers' precision grasping, considering grip failure involving slip and dynamic rotational stability. Comprehensive experiments across various objects, grip condition and types of fingers (PneuNet and commercial fingers) are conducted by examining the relationship between grasp parameters and model variables including coulomb friction, bulk stiffness, and dynamic stability. The findings demonstrate the model's utility in identifying optimal grip parameters that enhance the force capacity of soft fingers without causing dynamic instability. This research contributes to the development of more effective and stable soft robotic fingers for precision grasping tasks.**

I. Introduction

Soft fingers can grasp sensitive objects and handle geometry variations, especially with spherical or cylindrical objects where an enclosing grasp can be used [1], [2]. An enclosing or power grasp provides a large contact area between the finger and the object, making it well-suited for pick-and-place tasks in unobstructed environments [3].

However, soft fingers typically have reduced force capacity compared to rigid fingers [4], [5], limiting their payload capacity [6] and contact-rich tasks [7]. This limitation is significant when contact area is reduced: when grasping smaller or flat objects, or when a precision grasp, such as a fingertip or pinch grasp, is needed, e.g. to manipulate dexterously in cluttered environments [8]. Although three or more fingers can be used to improve grasp, objects that are smaller, not round, or in cluttered environments often require a parallel grasp with two fingers.

Ongoing work has explored increasing grasp strength through mechanical design: using stiffening elements [9], jamming techniques [10], incompressible actuating fluids [6], additional kinematic structure [11], and structured compliance [12]. While mechanical design is important, the force capacity is also affected by grip parameters such as the degree of actuation, robot grip pose, and finger distance.

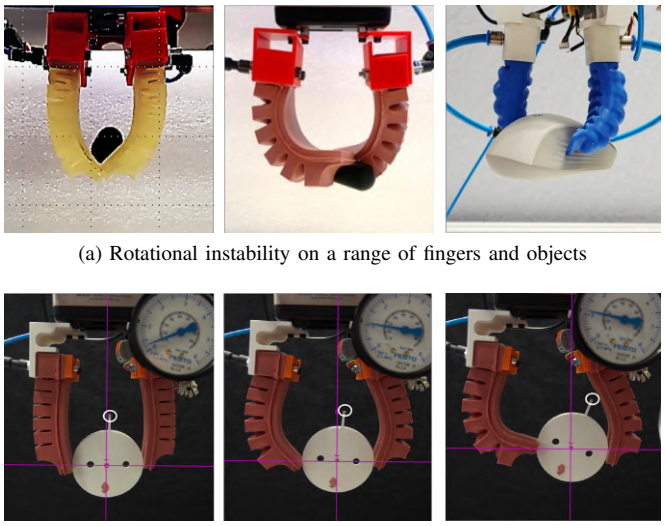

(a) Rotational instability on a range of fingers and objects

(b) Transition as pressure increases

Fig. 1: Rotational grasping instability of soft robotic fingers

Grasping instability can be observed on a range of fingers and objects in Fig. 1(a). When pressure increases, as seen in Fig. 1(b), the object begins to rotate, sometimes leading to slip at the contact points with the fingers. We observe that this rotational instability limits the ability to increase force capacity through increased pressure, and is affected by grasp parameters. Due to the complexity of soft fingers, tuning these grip parameters often relies on the experience of the users or computational simulation [13].

This rotational instability is influenced by both grip stability and slip. Grip stability has a wide range of definitions [14], [15]. Planar grip stability has been studied for force-closure [16], form-closure [17], and stiff-but-underactuated fingers [18]. However, these analyses assume the contact is a point and infinitely stiff, making them unrealistic for soft fingers. Although some approaches model finger compliance [15] for tendon-driven fingers [19] or spherical fingertips [20], modeling bulk motion of the fingers for optimizing grip parameters is needed to avoid rotational instability [8], as seen in Figure 1 and the attached video.

Slip is typically modeled with Coulomb friction in grasping [14], [21]. However, a Coulomb friction model is a point-contact model, raising questions about its applicability to a larger contact area in soft fingers. Friction models for spherical soft fingertips have been proposed [20], [22], [23], but have not been validated on general soft fingers.

Towards increasing the force capacity of soft fingers, this

[1]Department of Automation, Fraunhofer IPK, Berlin, Germany firstname.lastname@ipk.fraunhofer.de
[2]Department of Mechanical Engineering, UNIST,Ulsan, Korea jbbae@unist.ac.kr
Now, Prof. Joonbum Bae is with the School of Mechanical Engineering, Korea University, Seoul, Korea.

* denotes equal contribution. This research was supported by the MOTIE (Ministry of Trade, Industry, and Energy) in Korea, under the Fostering Global Talents for Innovative Growth Program related to Robotics (P0017311) supervised by the Korea Institute for Advancement of Technology (KIAT)

paper proposes a model for rotational stability and validates the bulk Coulomb model. Compared to friction modeling in soft fingers [21], [23], we examine the effect of contact area, pressure, and offset. This suggests that increasing normal force is the primary way to increase force capacity. However, increasing the normal force can lead to dynamic instability. Rotational instability is modeled by considering linear finger stiffness. Compared to classical grip stability [14], [16]–[19], this considers the rotational stability. These models are validated experimentally on a range of objects, grip conditions, and soft fingers (PneuNet [24] and commercial fingers). We then use the model to find grip parameters that improve force capacity.

In summary, we make the following contributions: 1. an analytical model of rotational stability in soft fingers' precision grasping relating the rotation angle to bulk stiffness; 2. empirically finding the relationship between grasp parameters and the model variables, validating Coulomb friction, and finding effects on bulk stiffness; 3. validating the model by comparing the force/angle between the model prediction and actual results; 4.introducing a simple case using the model for optimizing the grasping parameters.

II. Dynamic Grip Stability

We focus on precision grasping of lightweight objects in either the vertical (roll) or horizontal (yaw) plane . We define the rotational stability of soft fingers as the convergence of the angular displacement, $\theta \to 0$ over time and derive the stability conditions for the equilibrium point $\theta = 0$ using linear stability analysis of dynamic systems.

We assume that lightweight object's mass effects are negligible and that precision grasping leads to point contacts. As seen in Figure 2, the soft fingers are modeled as a 2D linear stiffness system, with stiffness parameters (k_n, k_t) in the normal and tangential directions, respectively, while ignoring torsional stiffness. The forces at the contact point are assumed to act symmetrically in the normal and tangential directions relative to the object's center of mass. The grasped object is characterized by its radius, r, and moment of inertia, I. The grip force of the finger in the normal direction is modeled by a relative spring displacement δ_n and the preload in the transverse direction is assumed to be 0.

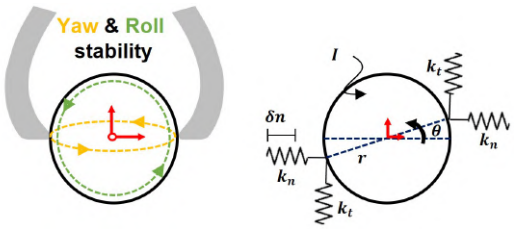

Fig. 2: Stiffness measurement of a planar soft finger, where the $\cdot_n$ and $\cdot_t$ denote normal and transverse, which change spatial direction for instability about the z or x axis.

A. Rotational dynamics

We model the pure rotation of the object as seen in Figure 2. The dynamics can be determined based on the energies of the system with Lagrangian mechanics. The kinetic energy T in the case of a pure rotation is given by $T = \frac{1}{2} I \dot{\theta}^2$, where I is the rotational inertia and $\dot{\theta} = d\theta/dt$. The potential energy of the system V is derived as

$$V = k_n(\delta_n - r(1 - \cos\theta))^2 + k_t(r \sin\theta)^2, \tag{1}$$

where r is the object radius, k_n and k_t are the stiffness in the respective directions, and δ_n is the preload displacement. We then find the equations of motion of

$$\begin{aligned} I\ddot{\theta} =& 2k_n r \sin\theta \delta_n - 2k_n r^2(1 - \cos\theta)\sin\theta \\ & - 2k_t r^2 \sin\theta\cos\theta. \end{aligned} \tag{2}$$

B. Linearized dynamics and stability

With a state vector $x = [\theta, \dot{\theta}]^T$, the convergence of $x \to 0$ can be considered using the control theory. When the system is dynamically stable around an equilibrium point (here, $x = 0$), it converges to that state over time from starting conditions near that state. When the system is dynamically unstable, it will diverge.

While the dynamics (2) are nonlinear, the local stability can be analyzed by linearizing them about $x = 0$, yielding a system matrix A of

$$A = \begin{bmatrix} 0 & 1 \\ 2rI^{-1}(k_n\delta_n - k_t r) & 0 \end{bmatrix}, \tag{3}$$

where $\dot{x} \approx Ax$. The stability of the linearized system is given by the eigenvalues of the A matrix, which can be found as

$$\begin{aligned} \lambda_{1/2} &= \pm\sqrt{2rI^{-1}(k_n\delta_n - k_t r)} \\ &= \begin{cases} \pm\sqrt{2rI^{-1}(k_n\delta_n - k_t r)}, & \text{for } k_n\delta_n > k_t r \\ \pm i\sqrt{2rI^{-1}(k_t r - k_n\delta_n)}, & \text{for } k_n\delta_n < k_t r \end{cases}. \end{aligned} \tag{4}$$

If the normal force at $\theta = 0$, denoted as the preload force $f_p = k_n\delta_n$, is greater than the product of transverse stiffness k_t and the object radius r, a pole will be in the right half-plane, indicating instability. This gives a dynamic stability condition around the equilibrium point $\theta = 0^\circ$ of

$$\underbrace{k_n\delta_n}_{f_p} < k_t r, \tag{5}$$

and we denote the force when this condition is violated as $f_p^i = k_t r$.

C. Rest position

As the preload force increases, at $f_p \geq f_p^i$ rotation away from $\theta = 0$ begins. However, the finger may converge to a rest angle $\theta \neq 0$, which we denote as θ_r. We find this rest angle from (2) by setting $\ddot{\theta} = 0$ and solving for θ. This system has solutions at $\theta_r = n\pi$ for $n \in \mathbb{Z}$, and

$$\theta_r = \arccos\left(\frac{f_p - k_n r}{k_t r - k_n r}\right) \tag{6}$$

when

$$\left|\frac{k_n\delta_n - k_n r}{k_t r - k_n r}\right| < 1. \tag{7}$$

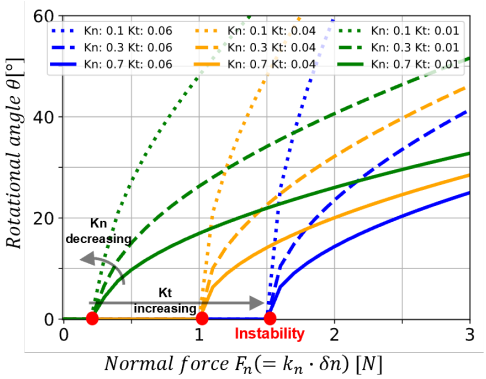

Fig. 3: Rest angle θ_r progression as k_n and k_t vary.

The progression of θ_r (6) as f_p increases is shown for selected system parameters in the Figure 3. It can be seen that the object begins to rotate when f_n exceeds the limit in (5). It should be noted that if the condition (7) is not satisfied, the progression of the rest position angle cannot be calculated and only the force f_p^i can be determined.

The comparison of these results for different k_n and k_t values can be seen in Figure. 3. As indicated by (5), the initiation of rotation depends on k_t, increasing as k_t increases. However, the slope after rotation is initiated decreases as k_n increases.

D. Rotation leading to slip

As the object rotates, the normal and transverse forces change, possibly leading to slip which often results in small objects flying from the gripper. Figure. 2 shows the normal force f_n and static friction force f_t, which from the nonlinear model can be defined as follows:

$$f_n = k_n(\delta_n - r(1-\cos\theta)) \quad (8)$$

$$= f_p - k_n r(1-\cos\theta) \quad (9)$$

$$f_t = k_t r \sin\theta, \quad (10)$$

where $f_p = k_n\delta_n$ is the preload force on the finger. These equations are connected by the Coulomb friction condition $|f_t| \leq f_n\mu$. With the assumption that the direction of the forces f_n and f_t doesn't change with rotation, the limiting case for the angle from which the slip begins can be determined by solving $f_t = \mu f_n$, which gives [25]

$$\theta_f = 2(\arctan(\frac{a \pm \sqrt{a^2+b^2-c^2}}{b+c}) + n\pi), n \in \mathbb{Z}, \quad (11)$$

where $a = k_t r, b = -\mu k_n r$ and $c = \mu f_p - \mu k_n r$. The angle θ_f indicates the rotation at which slip occurs. It follows that slip does not occur if the rest angle remains smaller than the critical angle $\theta_r < \theta_f$.

III. Friction Modeling

As friction force in grasping is essential for determining both slippage and measuring tangential direction stiffness, this section introduces the friction model in soft fingers. First the bulk Coulomb model of soft fingers is validated, then the slip and measurement of tangential direction of contact

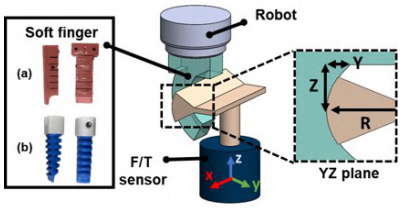

(a) Soft fingers(a: PneuNets [24], b : Soft-Gripping [29] and test object on the F/T sensor

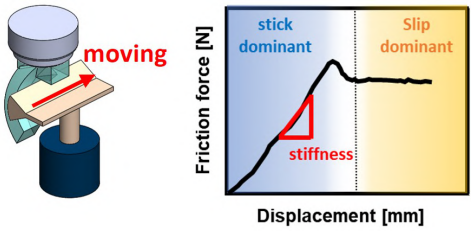

(b) Friction measurement motion and stick-slip transition results

Fig. 4: Friction measurement experimental setup

stiffness in rotation is modeled. Coulomb friction models slip as a violation of the condition $|f_t| < \mu f_n$, where $\mu \geq 0$ is the Coulomb friction coefficient, f_n is the normal force and f_t is the tangential force. These models are popular in soft robotics [9], [26], [27], and can also be made stochastic [21].

However, the Coulomb model is a point model, and it is unclear how it applies to larger contact areas. One reason for this is that the pressure distribution over the contact area not uniform, which can result in local slip, where local relative motion occurs before bulk slip [22]. Computational methods to estimate contact pressure have been proposed [28], but have not yet extended with frictional models. To investigate the accuracy of the bulk Coulomb friction model over soft grasp parameters (contact area, offset, pressure, material), we develop a test environment as shown in Figure 4.

Parameter name	Value
Pressure [bar]	0.4, 0.8, 1.2
Contact area [cm^2]	2.1(S), 4.2(M), 8.4(L)
Horizontal offset [mm]	0, 10, 20
Vertical offset [mm]	-20, 0, 20
Contact surface material friction	Ordinary, High

TABLE I: Parameters of the friction experiments

A. Coulomb model validation

The experimental setup seen in Figure 4, where cylinder segments of various arc lengths are 3D printed from Tough PLA with a radius of 30 mm. In this way, the contact area is controlled by the test object, provided the finger is in contact with the full arc of the object, which is verified visually per experiment. The test objects are mounted onto a Force/Torque sensor (ME-Meßsystem MP11, load limit 500N, 20Nm, sampling rate 125Hz) to allow measurement of the total normal and transverse force.

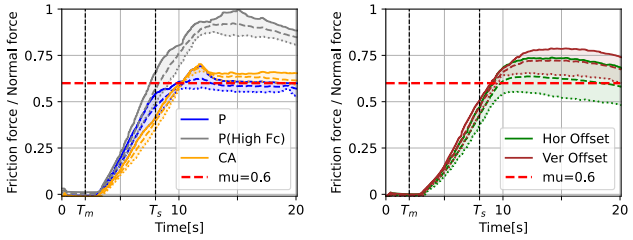

(a) Pressure, object(contact area, surface-high fc) (b) Horizontal and Vertical offset

Fig. 5: Variation in friction coefficient f_t/f_n, where the shaded region shows min/max values for specified grasp parameters. The reference value of $\mu = 0.6$ is shown in red.

Two different soft finger systems are prepared for verifying generalizability; Commercially available system, customized system. The commercially available finger system is manufactured by SoftGripping [29]. The customized pneumatic fingers are made with Wacker M4601 Elastosil(red fingers) and RT6245(transparent fingers), and the kinematic structure is based on PneuNets [24]. They are actuated by controlled pressure valves (VEAB-L-26-D9-Q4-V1-1R1, Festo), where a desired pressure is applied. The fingers are mounted on a Universal Robots UR10, which is used to initiate contact and load the fingers. We then compare five different parameters: pressure, contact area, relative position between finger and contact object (horizontal and vertical offset) and contact surface material. The range of parameters tested is shown in Table I. The high friction condition adds rubber to the surface of the test object.

For each set of parameters, the following experiment process is followed: (i) the finger is actuated in free space, (ii) the robot moves the finger into contact, (iii) contact along the entire test object is visually verified, (iv) linear motion in the positive y direction beginsT_m, with a velocity of 2mm/s and to a distance of 30mm, (v) the robot moves back to the initial pose. As the robot moves in the y direction, the total transverse force is measured as $f_t = f_y$ from the force/torque sensor. The total normal force is calculated as $f_n = \sqrt{f_x^2 + f_z^2}$, where f_z is assumed to be from asymmetrical contact pressure, not friction. Experiments are conducted for each parameter combination three times, with the mean value plotted.

Three phases of the friction forces can be identified, illustrated in Figure 4(b), right: the stick phase, where the fingertip is not moving while the robot moves with constant velocity, a transition region, and a constant friction phase as sliding occurs. In the stick phase, the slope of f_t represents the soft finger's bulk stiffness in y, k_y. After the transition phase, the asymptote in the sliding phase is taken as the friction coefficient μ.

The transverse force over normal force, f_t/f_n, can be seen in Figure 5, showing the min/max over each parameter in the shaded region. These results suggest that material choice dominates μ, which is less affected by other grip parameters. The vertical and horizontal offsets increase variation in μ due to changing the pressure profile, but these effects are bounded within $\mu \in [0.49, 0.77]$. While vertical and horizontal offset affect the effective friction coefficient, the variation in μ is $\pm 23\%$, and total friction force f_t can easily be dominated by changes in f_n. Consequently, the time interval ranging from T_m to T_s can be characterized as the stick phase, representing the measurable stiffness range.

IV. Experimental Validation of Stability Models

To validate the stability conditions in Section II, the stiffness properties are measured, then the rotation of test objects as pressure increases is shown for a range of grasp conditions. This is used to evaluate the models in Section II: when rotation away from initial orientation begins $f_p^i(k_n, k_t, r)$, the progression of rest angle θ_r, and when the rotation leads to slip at $f_p^s(k_n, k_t, r)$.

A. Measuring Finger Stiffness

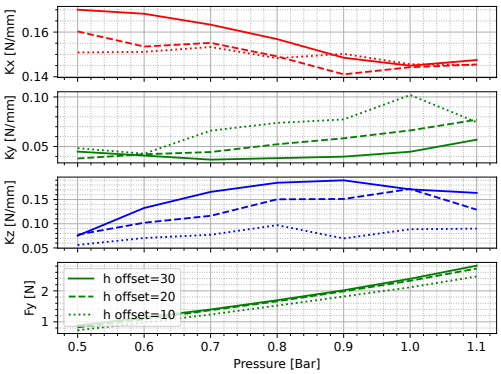

(a) Red fingers, horizontal offset, where rotation about x means $k_n = k_y$, $k_t = k_z$

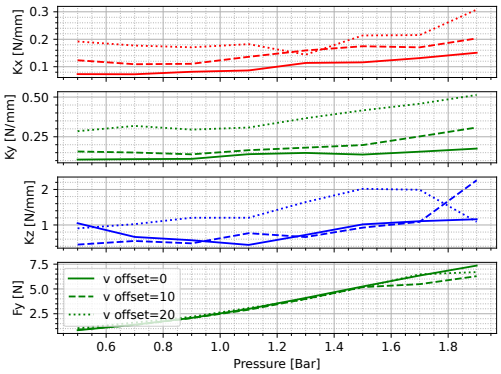

(b) Blue fingers, vertical offset, where rotation about z means $k_n = k_y$, $k_t = k_x$

Fig. 6: Finger stiffness and preload force over pressure and offset for the (a) red PneuNet fingers and (b) blue Soft Gripping fingers.

The stiffness of the finger is needed to validate the stability model. In order to measure this, an object is fixed on the force sensor and a single finger is mounted on the robot, as seen in Figure 4. A range of vertical or horizontal offsets are applied by moving the robot / gripper, then, for each offset, a range of pressures is applied. When the pressure is applied, the robot makes a small relative movements in the three spatial directions, pauses, and the forces are measured.

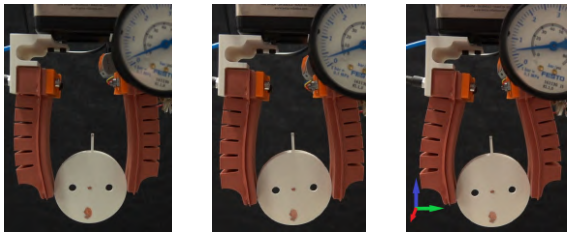

(a) Red fingers with 60mm object and horizontal offset 10mm (left), 20mm (mid), 30mm (right)

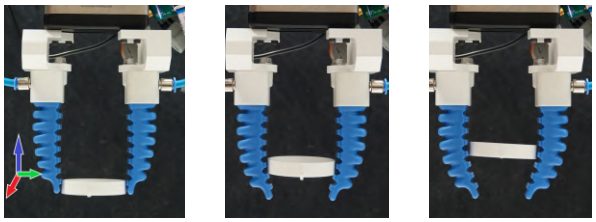

(b) Blue finger vert offset 0mm (left), 10mm (mid), 20mm (right)

Fig. 7: Grasp conditions for the rotation angle experiments, coordinates shown with x red, y green and z blue. In addition to the 60mm diameter object, 50 and 70 are used.

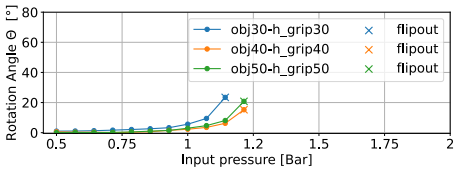

(a) Red fingers changing object diameter(r), fixed offset, instability about x

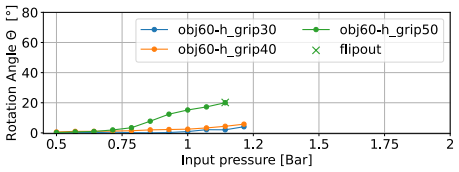

(b) Red finger, varying offset, instability about x

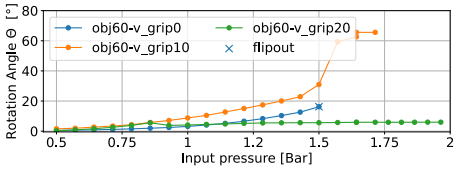

(c) Blue fingers, change in offset, instability about z

Fig. 8: Rotation angle over pressure for the different grip conditions shown in Figure 7.

For each motion, e.g. from x_0 to x_1, the forces measured at each position are f_0 and f_1, and the corresponding linear stiffness can be found as $k = \frac{f_1 - f_0}{x_1 - x_0}$. The size of the deltas is $[2, 2, 0.5]$mm (in x, y and z related to force sensor coordinate system) for the blue SoftGripping fingers [30], and $[2, 2, 1]$mm for the red PneuNet fingers [24] to avoid slip. These measurements are repeated at a range of pressures and robot pose offsets which correspond with the experiment conditions seen in Figure 7.

The results can be seen in Figure 6(a) for the PneuNets (red) and Figure 6(b) for the SoftGripping fingers (blue), under horizontal and vertical offsets as seen in Figure 7. A few general conclusions can be made: the offsets do not majorly change the relation between pressure and f_y. The stiffness in grip direction k_y is affected by pressure. For the red PneuNets, the vertical stiffness k_z increases as the offset increases, i.e. either a larger object is grasped or the parallel gripper is closed. However, k_x is not affected by offset. For the blue Soft Gripping fingers, the horizontal stiffness k_x is affected by vertical offset, increasing as the object is grasped 'deeper' in the fingers. k_z is large, and thus instability about x (where $k_t = k_z$) would not be expected.

B. Rotational measurements

To validate the rest angle that the object takes as grip force is increased, we use the test objects and grasp conditions shown in Figure 7, and take a video as the pressure is increased by steps. The red dots on the indicating stick and center can be tracked in the video software Tracker[1], and are used to find the change in rotation angle θ. To explore various experimental scenarios, we conducted experiments using two types of fingers: red and blue. Red fingers grasped objects horizontally, as depicted in Figure 7(a). We adjusted the spacing between fingers to vary the grasping configuration for the same object. Furthermore, to examine the influence of object size, we conducted experiments on objects of different sizes while maintaining a consistent relative distance (spacing between fingers - object size).

In the case of blue fingers, objects were grasped vertically, as shown in Figure 7(b). We conducted experiments with three different vertical offsets and measured angular displacement and instability based on pressure. Figure 8 shows the measured rest angle of both fingers with the respective offsets and flipout. The progression curves clearly depict the anticipated trend from the model Figure 3, with the flipout angle indicated at the corresponding point. Notably, the trend line varies according to the grip condition.

Figure 9(a) compares the predicted instability and the force when rotation begins. We set $5\,\mathrm{deg}$ as the start rotation angle for ease of measurement. Both fingers with zero offset grips have a lower RMSE between prediction and actual results $(0.39N)$ than offset grasping $(2.22N)$. Similary, Figure 9(b) compares the measured and predicted flipout angles. The zero offset grip more aligns closely to the model prediction of flipout angle, with RMSE values of $5\,\mathrm{deg}$ and $12\,\mathrm{deg}$ for the zero offset and offset-grips, respectively.

In all types of soft fingers, experimental conditions with zero offset grips show lower errors in both the force where rotation begins and the angle at which flipout occurs. The assumption that symmetrical forces act on both sides of the object, centered around its center of mass, resulting in zero net force in the vertical condition, match more closely to zero-offset grip. In contrast, with an offset grip, the net force in the vertical direction is existing.

Furthermore, our model effectively predicts the direction

[1]https://physlets.org/tracker/

of rotation, whether it occurs in the yaw or roll direction. As shown in equation (5) and Figure 6, the normal force f_n, corresponding to F_y, and k_t, where either k_x or k_z are considered to determine the direction of instability. While some cases show complex behaviors depending on object shape and grasping parameters, our model successfully predicts the rotational direction when the assumptions are met.

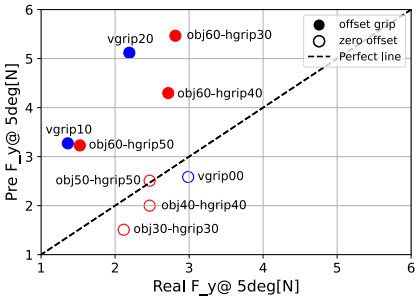

(a) Model instable force f_p^i vs force measured at 5 deg

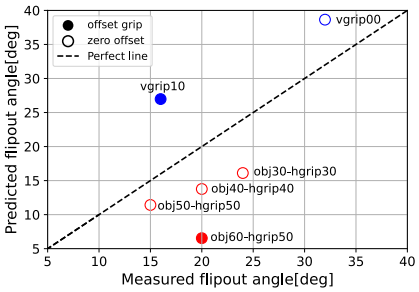

(b) Friction failure angle θ_f vs measured

Fig. 9: Comparing model predictions for: (a) model instability force f_p^i compared with force when object reaches 5 deg and (b) predicted flipout angle θ_f from (11) vs measured flipout angle.

C. Grip parameter optimization

Can the models be used to increase force capacity? This is investigated by experimentally finding the maximum pulling force in the vertical direction for the PneuNets, for a range of finger pressures and horizontal offsets. To measure force while allowing object instability, we modify the test objects to pass a string from the center, which is then fastened to the F/T sensor. In this way, if the grasp is unstable, the object will fly out and the resulting pull forces will be 0. The grasp conditions start as seen in Figure 10, and the robot moves vertically 30mm, and the maximum force f_z which occurs during this is measured. These experiments are repeated over a range of horizontal offsets and pressures, and the results can be seen in Figure 11.

The most stable grasp, expected from Figure 6, is with a horizontal offset of 30mm, which should be stable up to a grasp preload of $f_y = k_z r/2 = 4.8$N. We find that this grasp also provides the highest pull force.

V. Conclusion

In conclusion, this study explores the rotational dynamics in soft fingers' precision grasping. By identifying grip failure modes—slip and dynamic rotational stability—the research

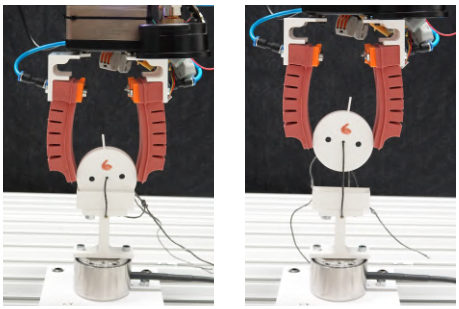

(a) Start, object in holder (b) Cable pulls as robot moves up

Fig. 10: Maximum pulling force setup, where the object starts in a holder and as the robot moves up, the cable pulls the object, transmitting forces to the F/T sensor while allowing instability

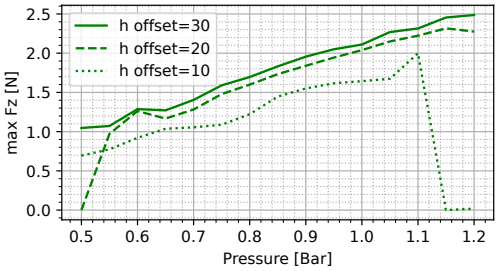

Fig. 11: Maximum pulling force results, where the highest offset achieves the highest grasp force.

lays the groundwork for optimizing grasp parameters. Analytical models developed in the study provide insights into factors influencing angular displacement, such as contact stiffness, normal force, and radius of the object. The models are validated for the pressure at which rotation begins and when frictional failure occurs in various gripping conditions. In scenarios of zero offset grasping within two different finger systems, where transverse forces were absent, the model demonstrated relatively accurate predictions. Nevertheless, when applied for predictive purposes overall, limitations in accuracy were evident.

The model faces limitations due to strong assumptions, such as neglecting the viscoelastic effects, gravity, surface properties of objects, and ignoring any transverse forces f_t. Moreover, the measurement required for all contact variables poses a significant challenge, and the model is only validated for single, small contact patches with the objects, leaving questions on its ability to extend to multi-contact grasps.

REFERENCES

[1] R. Ozawa and K. Tahara, "Grasp and dexterous manipulation of multi-fingered robotic hands: A review from a control view point," *Advanced Robotics*, vol. 31, no. 19-20, pp. 1030–1050, 2017.

[2] J. Hernandez, M. S. H. Sunny, J. Sanjuan, I. Rulik, M. I. I. Zarif, S. I. Ahamed, H. U. Ahmed, and M. H. Rahman, "Current Designs of Robotic Arm Grippers: A Comprehensive Systematic Review," *Robotics*, vol. 12, no. 1, p. 5, Jan. 2023.

[3] C. Piazza, G. Grioli, M. Catalano, and A. Bicchi, "A Century of Robotic Hands," *Annual Review of Control, Robotics, and Autonomous Systems*, vol. 2, no. 1, pp. 1–32, May 2019.

[4] M. Li, A. Pal, A. Aghakhani, A. Pena-Francesch, and M. Sitti, "Soft actuators for real-world applications," *Nature Reviews Materials*, vol. 7, no. 3, pp. 235–249, Nov. 2021.

[5] S. Liu, F. Wang, Z. Liu, W. Zhang, Y. Tian, and D. Zhang, "A Two-Finger Soft-Robotic Gripper With Enveloping and Pinching Grasping Modes," *IEEE/ASME Transactions on Mechatronics*, vol. 26, no. 1, pp. 146–155, Feb. 2021.

[6] O. Azami, K. Ishibashi, M. Komagata, and K. Yamamoto, "Development of hydraulically-driven soft hand for handling heavy vegetables and its experimental evaluation," in *2023 IEEE International Conference on Robotics and Automation (ICRA)*. IEEE, 2023, pp. 2577–2583.

[7] A. Billard and D. Kragic, "Trends and challenges in robot manipulation," *Science*, vol. 364, no. 6446, p. eaat8414, Jun. 2019.

[8] C. B. Teeple, T. N. Koutros, M. A. Graule, and R. J. Wood, "Multi-segment soft robotic fingers enable robust precision grasping," *The International Journal of Robotics Research*, vol. 39, no. 14, pp. 1647–1667, 2020.

[9] W. Park, S. Seo, J. Oh, and J. Bae, "A sensorized hybrid gripper to evaluate a grasping quality based on a largest minimum wrench," *IEEE Robotics and Automation Letters*, vol. 5, no. 2, pp. 3243–3250, 2020.

[10] K. Singh, S. Gupta, A. Khosla, and H. Furukawa, "Transforming Soft Robotics: Laminar Jammers Unlocking Adaptive Stiffness Potential in Pneunet Actuators," *ECS Journal of Solid State Science and Technology*, vol. 12, no. 4, p. 047007, 2023.

[11] J. Zhou, S. Chen, and Z. Wang, "A Soft-Robotic Gripper With Enhanced Object Adaptation and Grasping Reliability," *IEEE Robotics and Automation Letters*, vol. 2, no. 4, pp. 2287–2293, Oct. 2017.

[12] R. M. Hartisch and K. Haninger, "Compliant finray-effect gripper for high-speed robotic assembly of electrical components," *arXiv preprint arXiv:2301.08431*, 2023.

[13] M. A. Graule, C. B. Teeple, T. P. McCarthy, G. R. Kim, R. C. S. Louis, and R. J. Wood, "Somo: Fast and accurate simulations of continuum robots in complex environments," in *2021 IEEE/RSJ International Conference on Intelligent Robots and Systems (IROS)*. IEEE, 2021, pp. 3934–3941.

[14] M. A. Roa and R. Suárez, "Grasp quality measures: Review and performance," *Autonomous Robots*, vol. 38, no. 1, pp. 65–88, Jan. 2015.

[15] D. Prattichizzo, J. C. Trinkle, and B. Siciliano, "Grasping." 2008.

[16] J. C. Trinkle, A. O. Farahat, and P. F. Stiller, "Second-order stability cells of a frictionless rigid body grasped by rigid fingers," in *Proceedings of the 1994 IEEE International Conference on Robotics and Automation*. IEEE, 1994, pp. 2815–2821.

[17] A. Bicchi and V. Kumar, "Robotic grasping and contact: A review," in *Proceedings 2000 ICRA. Millennium Conference. IEEE International Conference on Robotics and Automation. Symposia Proceedings (Cat. No.00CH37065)*, vol. 1, Apr. 2000, pp. 348–353 vol.1.

[18] L. Birglen, T. Laliberté, and C. M. Gosselin, *Underactuated Robotic Hands*. Springer, 2007, vol. 40.

[19] M. Haas-Heger, G. Iyengar, and M. Ciocarlie, "Passive Reaction Analysis for Grasp Stability," Jan. 2018.

[20] H. Dong, C. Qiu, D. K. Prasad, Y. Pan, J. Dai, and I.-M. Chen, "Enabling grasp action: Generalized quality evaluation of grasp stability via contact stiffness from contact mechanics insight," *Mechanism and Machine Theory*, vol. 134, pp. 625–644, 2019.

[21] Z. Liu and R. D. Howe, "Beyond Coulomb: Stochastic Friction Models for Practical Grasping and Manipulation," *IEEE Robotics and Automation Letters*, 2023.

[22] A. Fakhari, M. Keshmiri, and I. Kao, "Development of realistic pressure distribution and friction limit surface for soft-finger contact interface of robotic hands," *Journal of Intelligent & Robotic Systems*, vol. 82, pp. 39–50, 2016.

[23] A. Fakhari, I. Kao, and M. Keshmiri, "Modeling and control of planar slippage in object manipulation using robotic soft fingers," *ROBOMECH Journal*, vol. 6, no. 1, pp. 1–11, 2019.

[24] P. Polygerinos, Z. Wang, J. T. Overvelde, K. C. Galloway, R. J. Wood, K. Bertoldi, and C. J. Walsh, "Modeling of soft fiber-reinforced bending actuators," *IEEE Transactions on Robotics*, vol. 31, no. 3, pp. 778–789, 2015.

[25] K. Zelator, "The equation asinx+bcosx=c and a family of cyclic heron quadrilaterals," p. 3, May 2008.

[26] N. Chavan-Dafle, R. Holladay, and A. Rodriguez, "In-Hand Manipulation via Motion Cones," Feb. 2019.

[27] F. R. Hogan, J. Ballester, S. Dong, and A. Rodriguez, "Tactile Dexterity: Manipulation Primitives with Tactile Feedback," in *2020 IEEE International Conference on Robotics and Automation (ICRA)*, May 2020, pp. 8863–8869.

[28] J. Masterjohn, D. Guoy, J. Shepherd, and A. Castro, "Velocity Level Approximation of Pressure Field Contact Patches," Jun. 2022.

[29] "The modular design system for flexible gripping." https://soft-gripping.com/, accessed: 2024-08-20.

[30] [Online]. Available: https://soft-gripping.com/